Research

New Phytologist

# Genetic analyses of embryo homology and ontogeny in the model grass *Zea mays* subsp. *mays*

**Hao Wu, Ruqiang Zhang and Michael J. Scanlon**

Plant Biology Section, School of Integrative Plant Science, Cornell University, Ithaca, NY 14853, USA

Authors for correspondence:
*Michael J. Scanlon*
*Email: mjs298@cornell.edu*

*Hao Wu*
*Email: haowu2021@gmail.com*

Received: *5 April 2024*
Accepted: *6 June 2024*

*New Phytologist* (2024) **243:** 1610–1619
**doi**: 10.1111/nph.19922

**Key words:** coleoptile, embryo, grasses, homology, maize, scutellum.

## Summary

- The homology of the single cotyledon of grasses and the ontogeny of the scutellum and coleoptile as the initial, highly modified structures of the grass embryo are investigated using leaf developmental genetics and targeted transcript analyses in the model grass *Zea mays* subsp. *mays*.
- Transcripts of leaf developmental genes are identified in both the initiating scutellum and the coleoptile, while mutations disrupting mediolateral leaf development also disrupt scutellum and coleoptile morphology, suggesting that these grass-specific organs are modified leaves.
- Higher-order mutations in *WUSCHEL-LIKE HOMEOBOX3* (*WOX3*) genes, involved in mediolateral patterning of plant lateral organs, inform a model for the fusion of coleoptilar margins during maize embryo development.
- Genetic, RNA-targeting, and morphological evidence supports models for cotyledon evolution where the scutellum and coleoptile, respectively, comprise the distal and proximal domains of the highly modified, single grass cotyledon.

## Introduction

Embryogenesis comprises the patterned growth and differentiation of the fertilized zygote, which culminates in the formation of lateral organs and the establishment of the general body plan. Many plant embryos make shoot/root apices and embryonic leaves (cotyledons) before the onset of seed quiescence, a signature endpoint of embryogenesis that interrupts organogenesis, which otherwise extends throughout the life cycle of land plants. The timing of seed quiescence is extremely variable within plant taxa, having co-evolved with the mode of seed dispersion (Kaplan & Cooke, 1997). Classical examples of plant embryogenic diversity include the eudicot *Arabidopsis*, which makes two cotyledons but no leaves before quiescence and maize, a monocotyledonous grass that initiates a single cotyledon and five or more foliar leaves before the seed desiccation. At another extreme, Rhizophoraceaen mangroves form embryos with well-developed shoots and elongated hypocotyls (embryonic stems) that dislodge from the mother plant and implant themselves as independent organisms into the sediment, without any quiescent delay in organogenesis (Kaplan & Cooke, 1997; Tomlinson, 2016). Among these morphological varieties and evolutionary questions, the homology of the single cotyledon of the grasses is a lingering problem in the evolution of plant development.

Embryogenesis in *Zea mays* subsp. *mays* may last 45–60 d, depending upon genotype and growth conditions. Following fertilization, the zygote divides to form a multicellular embryo that establishes apical–basal polarity by 4 d, comprising an apical embryo proper and a basal, transient suspensor that anchors the developing embryo in the seed (Kiesselbach, 1949; Abbe & Stein, 1954). At *c.* 7 d, the maize proembryo (Fig. 1a) undergoes histological patterning to form the embryonic epidermis (protoderm) and the internal cell layers (Kausch *et al.*, 2021). After 1–2 d, the shoot apical meristem (SAM) organizes on the apical face of the transition-staged embryo (Fig. 1b) and the scutellum initiates on the opposite side as the first embryonic lateral organ at *c.* 9 d after fertilization. The SAM comprises a pool of pluripotent stem cells that initiate the vegetative lateral organs of the maize shoot, although its role in the formation of the first maize embryonic organs is not clarified (Vollbrecht *et al.*, 2000; Takacs *et al.*, 2012; reviewed in Chandler, 2008 and Kaplan & Specht, 2022). Approximately 1 d after scutellum initiation, the SAM assumes an increasingly domed shape (Abbe & Stein, 1954) and the coleoptile initiates (Fig. 1c) as an emerging ridge apical to the SAM. In later stages, this ridge of initiating coleoptile will form a circular ring surrounding the SAM and all subsequent shoot embryonic organs. The first foliar leaf initiates from the SAM at Stage 1 (Fig. 1d) *c.* 11 d after pollination (DAP), whereafter the maize embryo typically initiates four additional leaf primordia before seed quiescence.

By comparison, embryogenesis in the eudicot *Arabidopsis* is truncated. Following the establishment of apical–basal polarity and histological layering, *Arabidopsis* embryos ultimately form paired cotyledons that comprise flattened, photosynthetic, leaf

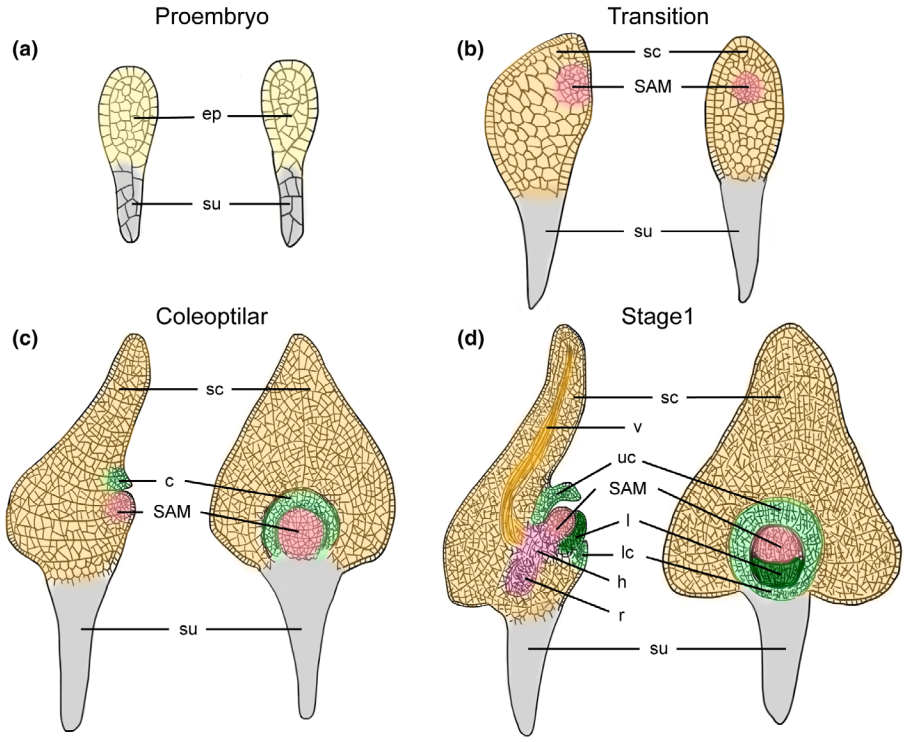


**Fig. 1** Developmental stages of maize embryogenesis. (a) Proembryo stage. The differentiation of the apical embryo proper and the basal suspensor; tissue layers organize. (b) Transition stage. The organization of the SAM and initiation of the scutellum. (c) Coleoptilar stage. The emergence of the coleoptile, the SAM forms a dome. (d) Stage 1. Emergence of the first foliar leaf. The coleoptile forms a ring-shaped structure with upper and lower coleoptile present in the longitudinal section. The vasculature tissue becomes histologically visible. For each panel, left and right images illustrate longitudinal median and paradermal views of the maize embryo, respectively. c, coleoptile; ep, embryo proper; l, leaf (dark green); lc, lower coleoptile (light green); SAM, shoot apical meristem (pink); sc, scutellum (yellow); su, suspensor (grey); uc, upper coleoptile (light green); v, vasculature (orange); h, hypocotyl (mesocotyl, light pink); r, root (dark pink).

homologs, and a SAM before seed desiccation (Kaplan & Cooke, 1997). Whereas the maize coleoptile is likewise laminate and photosynthetic (Langdale *et al.*, 1988), it fuses to form a protective sheath surrounding the emerging seedling and thereby functions to protect the germinating plantlet (Boyd, 1931; Kiesselbach, 1949). By contrast, the mature maize scutellum is a spade-shaped glandular organ of uncertain leaf homology located adjacent to the endosperm that functions as a haustorium to digest the endosperm and nourish the seedling (Weatherwax, 1920). Thus, the homology of the single cotyledon of monocot grasses is uncertain.

Cotyledonary number has been a pivotal component of plant classification for > 300 yr (Ray, 1686). In addition to the plethora of conforming monocotyledonae and dicotyledonae containing one or two embryonic leaves, respectively, there are monocots with two or more cotyledons and eudicots with no cotyledons, while others are polycotyledenous and harbor three or more cotyledons (Fu, 2024, and references therein). Cotyledons are proposed to have evolved in seed-bearing plants only, via the modification of ancestral foliar leaves (Niklas, 2008). Evidence for the homology of leaves and cotyledons includes their position in the body plan, proximity to the SAM, similar morphology and growth patterns, and the existence of intermediate leaf-cotyledon morphologies when these structures differ markedly at maturity (Kaplan, 1984; Kaplan & Cooke, 1997).

Dicotyledony is proposed to be ancestral to monocotyledony (Dean, 2002; reviewed in Chandler, 2008), although others have argued against the homology of eudicot and monocot cotyledons and consider them to be evolutionarily unrelated embryonic organs (Burger, 1998). Analyses of the paleodicot *Nymphaea* suggest that these basal angiosperms, which diverged earlier from the lineage leading to eudicots and monocots, contain either a single cotyledon or perhaps two fused cotyledons, leading to controversy as to their monocotyledonous or dicotyledonous nature (Titova & Batygina, 1986; Tillich, 1990). Models exist for the evolution of monocotyledony via the union of the two cotyledons in a dicotyledenous ancestor (syncotyly; Sargent, 1903; Haines & Lye, 1979), while others suggest that the splitting or duplication of an ancestral single cotyledon generated dicotyledony (reviewed in Chandler, 2008).

The ontogeny and homology of the grass cotyledon is particularly unresolved. Morphological models differ as to whether the single grass cotyledon comprises the scutellum, the coleoptile, or a composite organ containing the conjoined scutellum and coleoptile as the single cotyledon (Weatherwax, 1920; Boyd, 1931; Kaplan & Specht, 2022). In the first model, the scutellum comprises the haustorial cotyledon, whereas the coleoptile is a modified foliar leaf (Weatherwax, 1920). Boyd (1931) suggested that the coleoptile is the maize cotyledon, and the scutellum is an evolutionary novelty of grasses. A bipartite model proposes that the haustorial scutellum and the emergent, sheathing coleoptile comprise the distal and proximal domains of a single, united grass cotyledon (Kaplan & Specht, 2022). Transcriptomic analyses of embryonic SAM ontogeny provide support for the homology of the scutellum and coleoptile as modified leaves comprising a single, bipartite, grass cotyledon (Takacs *et al.*, 2012; Wu *et al.*, 2024), although genetic evidence in support of any one of these disparate models has been sparse.

This study combines higher-order genetic analyses of mutations disrupting leaf mediolateral patterning with multiplexed analyses of leaf transcript localizations to investigate the homology and ontogeny of the maize cotyledon. The data suggest that

both the scutellum and coleoptile are leaf homologs. A mechanistic model for the fusion of the coleoptile margins to form a sheathing tube that protects the germinating seedling is proposed. Our transcriptional and genetic data support models where the grass cotyledon is a bipartite fused organ, comprising a distal, haustorial scutellum and a proximal, sheathing coleoptile.

## Materials and Methods

### Plant materials and growth conditions

Stocks of the *Zea mays* L. subsp. *mays* inbred line B73, the first maize variety to be genome-sequenced (Schnable *et al.*, 2009), and the *narrow sheath* (*ns*) 1 : 1 line were grown in the Gutermann glasshouse facility at Cornell University, Ithaca, NY, USA. Specifically, the *ns* 1 : 1 line segregates one or two wild-type (WT), wide-leaved *NS1+/ns1 ns2/ns2* plants, and 1/2 *ns1/ns1 ns2/ns2* double mutants with narrow leaves (Scanlon *et al.*, 1996) rendered by null mutations in the paralogous *WUSCHEL*-like *HOMEOBOX3* (*WOX3*) transcription factor genes *NS1* and *NS2* (Nardmann *et al.*, 2004). Transition-staged, coleoptilar-staged, Stage 1, and Stage 2 embryos were collected at 8–9 DAP, 10–11 DAP, 12–13 DAP, and 14–15 DAP, respectively. Seeds from the *ns* 1 : 1 line were planted in soil consisting of a 1 : 1 mixture of Turface and LM111 in Percival A100 growth chamber at Weill Hall, Cornell University, Ithaca, NY, with set conditions, comprising 29.4°C : 23.9°C; 16 h : 8 h; day : night; and humidity 50%. Seedlings were collected at 7 d after planting for comparisons of WT and *ns1 ns2* mutant coleoptiles.

### Histology and conventional *in situ* hybridizations

Developing kernels and 7 d after planting seedlings were fixed in FAA, dehydrated, cleared, embedded in Paraplast™ (McCormick Scientific, Berkeley, MO, USA), and sectioned/stained as described previously (Jackson, 1991; Leiboff *et al.*, 2016; Satterlee *et al.*, 2023). For *in situ* hybridizations, gene-specific probes were synthesized, hybridized, and visualized as described (Jackson, 1991); primers for probe synthesis were adapted from Satterlee *et al.* (2023). Samples were photographed under light microscopy with a Z1-Apotome (Carl Zeiss, Oberkochen, Germany); Toluidine Blue O-stained sections were prepared as described (Strable *et al.*, 2020).

### Multiplexed *in situ* hybridization (RNA targeting)

Multiplexed *in situ* hybridization was performed on the 10× Genomics™ Xenium™ Platform for RNA targeting, at the Memorial Sloan Kettering Cancer Center, NY, following the manufacturer's protocol. The gene probe design, embryo tissue sections, sample processing, and data analysis are described previously (Wu *et al.*, 2024). The data were visualized on Xenium Explorer v.1.3., which enables dot detection imaging in addition to transcript-density plots that were based on spatial transcript abundance for quantitative *in situ* hybridization imaging.

### Elliptic Fourier transform of embryo boundary shape

Mature seeds of WT and *ns1 ns2* double mutants were photographed from the germinal face of the kernel; digital images from 21 seeds per genotype were generated. The coordinates of the two-dimensional embryonic boundaries were determined as described previously (Leiboff *et al.*, 2016) by WebPlotDigitizer v.4.6 (https://automeris.io/WebPlotDigitizer) with the following changes and details. An embryo boundary shape image was created by Matlab to conserve aspect ratios of the embryo shape, connecting neighboring coordinates to fill the borders, and was saved in jpg format.

The embryo boundary shape images were then converted and saved into 24 bitmap format using Microsoft Paint v.11.2302.19.0. Chain codes were assigned to the binary images (black background and white object) of the seed samples, to construct the outline-based morphology of the seed embryos. The chain codes that describe the seed embryo shape geometry information were determined by the default setting of the software Shape v.1.3 (Iwata & Ukai, 2002). To reconstruct the embryo shape outline, the assigned chain codes were converted into shape variables in the form of elliptic Fourier coefficients (EFC) using the first 20 harmonics (each harmonic consisting of four values) and then normalized using 77 elliptic Fourier descriptors.

The variations derived after EFC of the chain code data were summarized using principal component analysis (PCA; Iwata & Ukai, 2002). Only the significant principal components derived from the analysis were included. PCA was performed from the normalized EFC, wherein the scores in each component were used to describe the embryo shape characters.

To test for significant differences in the shape of the WT and *ns* mutant embryos, pair-wise Euclidean distances were computed from the matrix of five principal component scores from the combined PCA of all embryos, using the NPMANOVA multivariate analysis tool (Anderson, 2001). NPMANOVA is a non-parametric analog of multivariate analysis of variance (MANOVA), which calculates an *F*-test of variance between the two samples, computed from 999 replicate permutations of group membership. A scatter plot was generated using the first two principal component scores to visualize the distributions of embryo shape variations (Rohatgi, 2022).

### Quantitative comparison of coleoptiles in wild-type and *ns1 ns2* seedlings

Coleoptiles were collected from 7 d after planting seedlings of the *ns* 1 : 1 line (described in Materials and Methods section) including 12 WT and 12 *ns1 ns2* mutant seedlings. Two transverse sections for each plant were photographed (48 sections in total). The arc length connecting the two vascular bundles on the fused side of the coleoptile (*F*) and from the scutellum side of the coleoptile (*S*); the thickness of the tissue at the fused site (*b*) and at the two vascular bundles (*a1* and *a2*), as well as the major and minor axis of stem–leaf complex (*C* and *D*, respectively) were calculated. Normalized relative arc length (*Ar*) and tissue thickness

($Tr$) at the coleoptile fusion site were calculated using the following equations:

$$\text{Relative arc length at fused site } (Ar) = \frac{F}{F+S}$$

$$\text{Relative thickness at fused site } (Tr) = \frac{2b}{a_1 + a_2} \times \frac{C}{D}$$

The mean value of $Ar$ and $Tr$ of the WT and *ns1 ns2* were compared via Student's *t*-test by JMP Pro v.17.0 (SAS Institute, Cary, NC, USA).

## Results and Discussion

### Mutations disrupting mediolateral leaf development have equivalent effects on the scutellum and coleoptile

Mutations in homologous genes are predicted to have similar effects on homologous organs, although genetic redundancies can complicate such analyses. Solo mutations in either *NARROW SHEATH1* (*NS1*) or its paralog *NS2* have no detectable leaf phenotypes, although *ns1 ns2* double mutations condition a significant decrease in the width of the proximal regions of all foliar leaves and leaf-like organs of the maize inflorescence (Scanlon *et al.*, 1996; Scanlon & Freeling, 1998). However, previous studies (Scanlon *et al.*, 1996; Scanlon & Freeling, 1998) reported no obvious morphological effects of *ns1 ns2* mutations on either the scutellum or the coleoptile. Thus, these embryonic organs were quantitatively re-examined.

Elliptic Fourier transform methods use multiple sinusoid harmonics to reproduce highly complex shapes that can be separated by principal component analyses to identify subtle shape variations (Claude, 2008; Leiboff *et al.*, 2016). These methodologies revealed that mature WT and *ns1 ns2* mutant seed exhibit statistically significant differences in scutellar shape, such that the double-mutant scutellum is narrower at the base and less ovate than in WT siblings (Fig. 2a,b).

Grass coleoptiles have paired vascular bundles that are located at opposing sides of the coleoptile and arranged 90 degrees from the axis of coleoptile fusion at the embryo face (modeled in Fig. 2d,e). We tested predictions that the arc length connecting the two vascular bundles on the fused side of the *ns1 ns2* mutant coleoptile is shorter than in WT siblings (Fig. 2d). Arc lengths in normal and mutant coleoptiles ($n = 48$) were calculated and normalized to the circumferences, revealing significantly shorter vascular arc lengths in *ns1 ns2* mutants (WT $= 0.532 \pm 0.0037$; *ns1 ns2* $= 0.520 \pm 0.0029$; $P = 0.01$). Thus, mutations in the *ns1 ns2* duplicate genes disrupt mediolateral development in both the scutellum and coleoptile, in addition to their effects on all foliar leaves generated in the embryo (Scanlon & Freeling, 1998).

The margins of the growing maize coleoptile eventually fuse, forming an elliptical sheathing structure that surrounds and protects the young leaves and underlying SAM during seedling germination through the soil (Kiesselbach, 1949; Abbe & Stein, 1954). Coleoptilar fusion is complete by late Stage 1 in WT embryos (Abbe & Stein, 1954), although the edges of the *ns1 ns2* double-mutant coleoptile are not yet joined as late as Stage 2 (Fig. 3a,b,e,f). Later comparisons of germinated seedlings 7 d after planting reveal coleoptilar fusion in both WT and *ns1 ns2* mutant siblings, although the fusion site appears thicker in the mutant seedlings (Fig. S1i,j). Indeed, normalized quantitative measures of tissue thickness in WT vs *ns1 ns2* double-mutant seedlings ($n = 48$; see Materials and Methods section) revealed significantly thicker fusion sites in the mutant coleoptile (Fig. 2e; WT $= 0.429 \pm 0.0223$; *ns1 ns2* $= 0.561 \pm 0.0160$; $P < 0.0001$).

### Ontogeny of maize coleoptile fusion

*NS1* is expressed in the margins of leaf primordia where it functions in mediolateral expansion, whereas *FLOWERING PROMOTING FACTOR1-Like* (*FPF1-Like*), a gene of unknown function in maize, is co-expressed with *NS1* at primordial leaf margins (Satterlee *et al.*, 2023). *FPF1-Like* expression requires NS1/2 function (Satterlee *et al.*, 2023) and is used as a marker of marginal growth in maize leaves, although unlike *NS1/2*, its expression extends internally from the leaf margin toward the middle domain. Transverse sections of transition-staged maize embryos show that *NS1* transcripts accumulate at the periphery of the embryo proper region flanking the SAM (Fig. 4a), coincident with the initial morphogenesis of the scutellum. At Stage 1, *NS1* transcripts localize to the marginal edges of the growing coleoptile; no expression is noted in the scutellum at this stage (Fig. 4b,c). The coleoptilar margins of WT embryos fuse during late Stage 1; *NS1* transcripts are still detected in the fused coleoptile margins (Fig. 4c), as well as in the growing margins of the newly emerged Leaf 1 and in two foci in the SAM periphery corresponding to the leaf and right margins of the incipient Leaf 2 primordium.

*FPF1-Like* is also expressed in a lateral band within the embryo proper of the transition stage embryo during scutellum initiation (Fig. 4d), and in the growing edges of the coleoptile before they fuse to cover the embryonic shoot apex (Fig. 4e). At late Stage 1 however, *FPF1-Like* transcripts are not detected in the postfusion coleoptile (Fig. 4f) although signal is still detected in the unfused Leaf 1 primordial margins. Like *NS1*, *FPF1-Like* transcripts are not detected in the scutellum after the transition stage (Fig. 4e,f; Takacs *et al.*, 2012). In summary, the leaf primordial markers *NS1* and *FPF1-Like* are expressed in both the initiating scutellum and in the developing coleoptile, the first two embryonic lateral organs of grasses.

The maize *NS1/NS2* paralog *WOX3a* functions during mediolateral leaf development (Satterlee *et al.*, 2023). Higher-order mutant *ns1 ns2 WOX3a/wox3a* heterozygous plants are described as *very narrow sheath* (*vns*), wherein the leaf mediolateral domain deletion is more severe than in *ns1 ns2* double mutants. Triple-mutant *ns1 ns2 wox3a* leaves, however, are severely truncated mediolaterally, thus revealing dosage effects of WOX3 function (Satterlee *et al.*, 2023). We used the Xenium™ RNA-targeting strategy (Wu *et al.*, 2024) to compare the relative transcript accumulation densities of *WOX3a* and *NS1* in microtome sections of developing maize embryos. Unlike conventional *in situ* hybridization analyses, Xenium™ enables measurements

New Phytologist

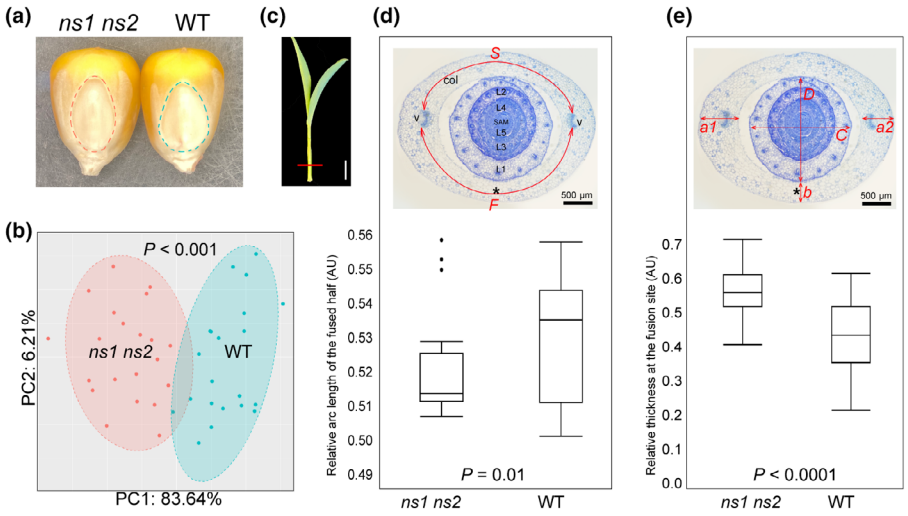


**Fig. 2** *ns1 ns2* mutations disrupt scutellum and coleoptile patterning in maize. (a) Comparison of the scutellum of mature seed from wild-type (WT) and *ns1 ns2* plants. The red and blue dashed lines mark the circumference of the WT and *ns1 ns2* scutellum. (b) Quantitative comparison of mature-seed scutellum shape via elliptic Fourier transform. A principal component analysis (PCA) shows a significant separation between WT and *ns1 ns2* scutellar shape ($P < 0.001$). (c) WT seedlings at 7 d after planting; the red line marks transverse section plane of the panel (d, e). Bar, 1 cm. (d) Quantitative comparison of the relative arc length of the fused half of the WT and *ns1 ns2* double-mutant coleoptile. *F* portrays the arc length connecting the two vascular bundles on the fused side of the coleoptile; the fusion site is marked by *. *S* portrays the arc length connecting the two vascular bundles on the scutellum side of the coleoptile (bar, 500 μm). Boxplots show that the *ns1 ns2* coleoptile has a significantly shorter arc length of the fused side of the coleoptile than the WT counterpart ($P = 0.01$). (e) Quantitative comparison of the relative tissue thickness at the coleoptile fusion site (*). (b) represents the thickness of the tissue at the coleoptile fusion site; *a1*, *a2*, equals the thickness of the tissue at the two vascular bundles (dark blue circles); (c, d) portray the major and minor axes of stem–leaf complex, respectively (bar, 500 μm). Boxplots show the *ns1 ns2* coleoptile is significantly thicker at the fusion site than WT counterparts ($P < 0.0001$); the middle line reflects the median value, the box shows the 25th and 75th percentile, and the whiskers reflect 1.5 times the interquartile range.

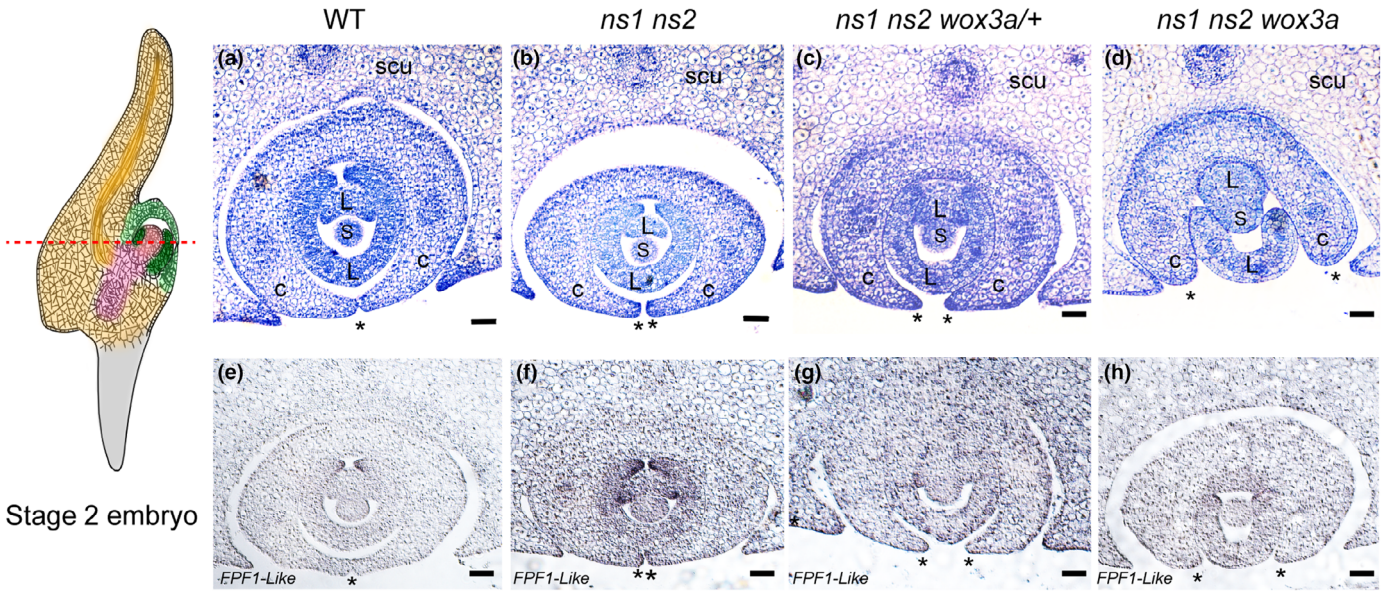


**Fig. 3** Embryonic coleoptile phenotypes of the *wox3* higher-order mutants of maize. (a–d) Toluidine blue stained and (e–h) *FLOWERING PROMOTING FACTOR1-Like* (*FPF1-Like*) *in situ* hybridizations of transverse sections of the wild-type (WT) (a, e) and *ns1 ns2* (b, f), very narrow sheath (*ns1 ns2 wox3a*/+; c, g), and triple mutant (*ns1 ns2 wox3a*; d, h) shoot apex at Stage 2. Cartoon at left shows approximate level of transverse sections (dashed red line) of samples. Asterisks (*) mark the two edges of the fused (a, e) and unfused (b–d; f–h) coleoptiles. c, coleoptile; L, leaf; S, SAM; scu, scutellum. Bars, 100 μm. *WOX3*, *WUSCHEL-LIKE HOMEOBOX3*. Colors in the Stage 2 embryo cartoon: scutellum (yellow); vasculature (orange); coleoptile (light green); leaf (dark green); suspensor (grey); SAM, root and hypocotyl (pink).

of transcript density that yield quantitative hybridization data, where the intensity of the signal corresponds to transcript abundance (Wu *et al.*, 2024).

These analyses reveal that *NS1*, but not *WOX3a*, is detected in the initiating scutellum at the transition stage (Fig. 5a,d), whereas both paralogs are detected in the initiating coleoptile (Fig. 5b,e,

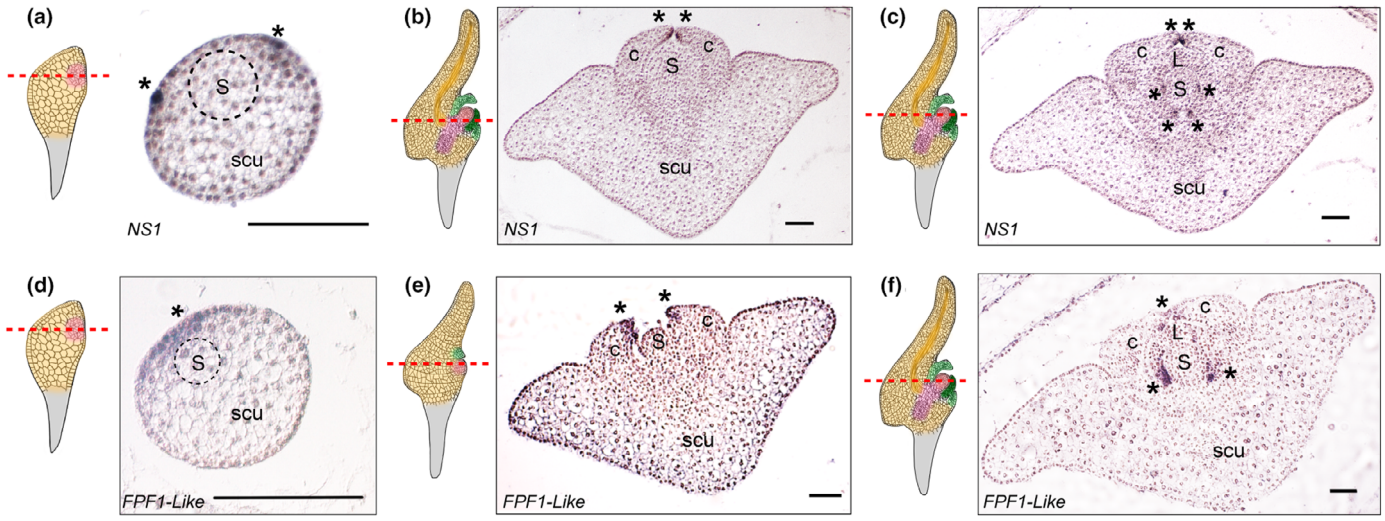


**Fig. 4** *In situ* hybridization of *NARROW SHEATH1* (*NS1*) and *FLOWERING PROMOTING FACTOR1-Like* (*FPF1-Like*) during maize embryo development. Transverse sections of transition-staged embryos hybridized to antisense probes from *NS1* (a) and *FPF1-Like* (d), and of *NS1* (b, c) and *FPF1-Like* (e, f) before (b, e) and after (c, f) coleoptilar fusion. The red dashed lines on the embryo models mark the approximate section planes of the micrograph images on the right. Asterisks (*) mark the *in situ* hybridization signal maxima; c, coleoptile; L, leaf; S, SAM; scu, scutellum. Bars, 100 µm. *WOX3*, *WUSCHEL-LIKE HOMEOBOX3*. Colors in the embryo cartoons: SAM, root, hypocotyl (pink); scutellum (yellow); suspensor (grey); coleoptile (light green); leaf (dark green); vasculature (orange). Cartoons in (a, d) are Transition stage; (e) is Coleoptilar stage; (b, c, f) are Stage 2.

g–k) and in the Stage 1 coleoptile (Fig. 5c,f), as well as in the first leaf primordium at Stage 1 (Fig. 5c,f). Consistent with prior descriptions (Satterlee *et al.*, 2023), *WOX3a* accumulation is generally more widespread and at lower density than *NS1*. Specifically, *NS1* expression is strong at the tip of the initiating coleoptile (Fig. 5b), while *WOX3a* is expressed at lower density in the coleoptile tip and at two other locations in the equivalently staged embryo, correlated with the initiation sites of the lower coleoptile and Leaf 1 (Fig. 5e). Notably, *WOX3a* transcripts accumulate in epidermal and internal tissues of the coleoptile, whereas *NS1* is mainly restricted to the epidermis (Fig. 5k). At Stage 1, *NS1* expression density is high in the upper and lower coleoptile and in the leaf (Fig. 5c), while *WOX3a* expression partially overlaps that of *NS1* but is expanded to include the region of the SAM predicted to mark the incipient Leaf 2, an area that is not marked by *NS1* expression (Fig. 5f). Furthermore and as described in Fig. 4, no *NS1* expression is detected in the scutellum after the transition stage.

Unlike foliar leaves containing a single prominent midvein, the maize coleoptile harbors two equivalently large vascular bundles at opposing sides of the fused cylindrical structure (Figs 2c,d, S1i). Whereas the *wox3* double-mutant *ns1 ns2* has quantifiable effects on the thickness of the coleoptile fusion site and its distance from the major veins (Figs 2c,d, S1b,f,j), triple-mutant *ns1 ns2 wox3a* leaves and coleoptile are severely truncated and the coleoptile fails to fuse, thereby partially exposing the germinating shoot (Figs 3d,h, S1d,h,i). *WOX3a* function is dosage sensitive (Satterlee *et al.*, 2023), such that *ns1 ns2 wox3a/WOX3a* seedlings exhibit coleoptile and leaf truncation phenotypes (termed *very narrow sheath*) that are intermediate between *wox3* double and triple mutants (Figs 3c,g, S1c,g,k).

Some have proposed that the grass coleoptile evolved via fusion of the two cotyledons in a dicot ancestor; unification was thought to occur at the margins, thereby combining two phytomers at their respective margins (reviewed in Cronquist, 1988; Bossinger *et al.*, 1992; Scanlon & Freeling, 1998). Our new analyses of higher-order *wox3* mutants do not support such a model, but instead suggest that coleoptilar fusion happens at the marginal domains of a single phytomer with two very prominent '-mid-veins' (Fig. 6a). Genetic deletion of the marginal domain by *ns1 ns2* double mutations leads to the fusion of the outer-lateral domains of the truncated, *ns* mutant coleoptile (Fig. 6b). In this model, the lateral domain comprises both an inner-lateral and an outer-lateral domain, as indicated by dosage-dependent WOX3a function (Satterlee *et al.*, 2023). Loss of either the outer-lateral domain in *very narrow sheath* mutants, or the complete outer- and inner-lateral domains in *wox3* triple mutants, results in circumferentially shortened, unfused, mutant coleoptiles that fail to surround the embryonic shoot (Fig. 6c,d).

## Homology of the maize cotyledon

Morphological models differ as to whether the single grass cotyledon comprises just the scutellum, the coleoptile, or is a composite organ comprising the conjoined scutellum and coleoptile (Weatherwax, 1920; Boyd, 1931; Bossinger *et al.*, 1992; Scanlon & Freeling, 1998; Chandler, 2008; Kaplan & Specht, 2022).

The scutellum and coleoptile are the first-formed structures of the grass embryonic shoot; their shared positions on the same side of the shoot apex suggest a single organ, since successive leaves initiate in distichous phyllotaxy (alternate opposite and in two ranks) in the grasses (Kaplan & Specht, 2022). The bodies of the

New Phytologist

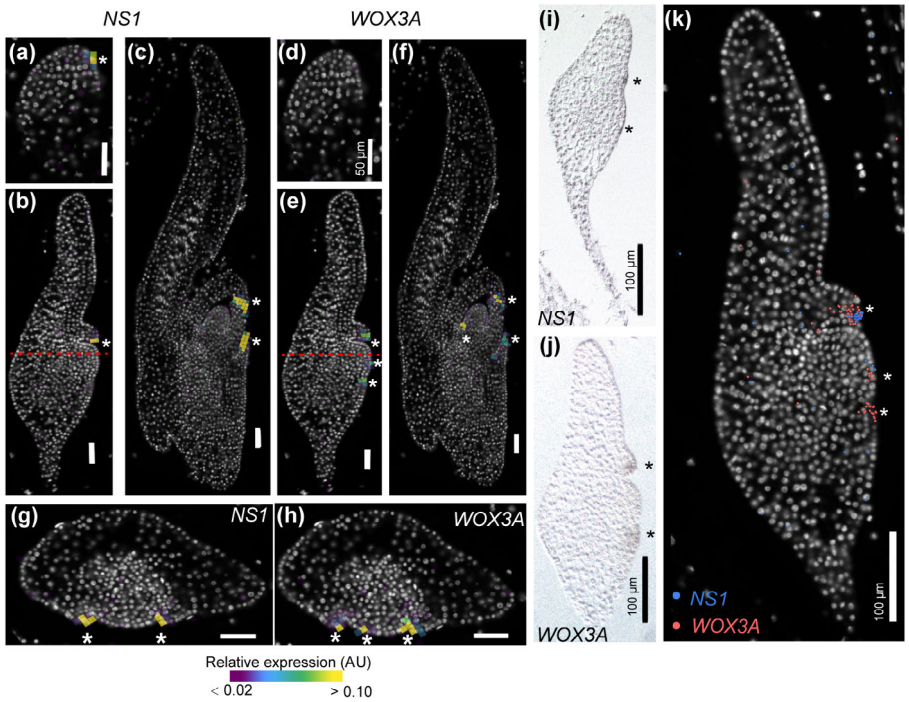


**Fig. 5** Multiplex *in situ* hybridization of *NARROW SHEATH1* (*NS1*) and *WOX3A* during maize embryogenesis. *NS1* expression density map of longitudinal embryo sections at the transition stage (a), coleoptilar stage (b), and Stage 1 (c). Asterisks (*) denote sites of *NS1* accumulation (a–c, g and i) or *WOX3A* accumulation (d–f, h, and j). Upper asterisk (*) in (k) denotes *NS1* and *WOX3A* accumulation; lower two asterisks (*) denote *WOX3A* accumulation. The red dash lines in (b, e) mark the approximate planes of transverse section of the embryos shown in (g, h). Bars, 50 µm. *WOX3A* expression density map of embryo longitudinal sections at the transition stage (d), coleoptilar stage (e), and Stage 1 (f). Bars, 50 µm. *NS1* (g) and *WOX3A* (h) expression density maps of transverse embryo sections at the coleoptilar stage. Bars, 50 µm. AU, arbitrary units. Conventional *in situ* hybridizations of *NS1* (i) and *WOX3A* (j) in longitudinal sections of coleoptilar-staged embryos. Bars, 100 µm. (k) *NS1* (blue dots) and *WOX3A* (red dots) expression in longitudinal sections of coleoptilar-staged embryos. Bar, 100 µm. *WOX3*, *WUSCHEL-LIKE HOMEOBOX3*.

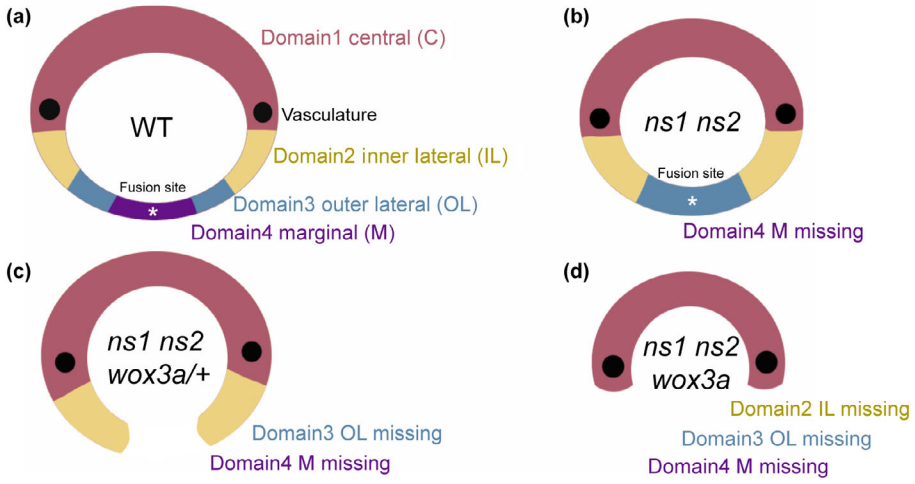


**Fig. 6** Model for WOX3-mediated patterning of coleoptile growth and fusion in maize. (a) Wild-type (WT) coleoptile includes four mediolateral domains, comprising the central (maroon), inner lateral (IL, yellow), outer lateral (OL, blue), and marginal (purple). The two edges of the WT coleoptile fuse at the marginal domains. (b) The *ns1 ns2* mutations remove the marginal domains; coleoptile fusion happens in *ns1 ns2* mutants at the OL domains, causing shorter coleoptile arc lengths and a thicker coleoptile fusion site. The *ns1 ns2 wox3a/+ very narrow sheath* (*vns*) mutant removes the OL domain *and* marginal domain. (c) The two edges of the *vns* coleoptile fail to fuse, leaving a gap between edges of the IL domains. (d) The *ns1 ns2 wox3a* triple mutant deletes the IL, OL, and marginal domains; the two edges of the coleoptile fail to fuse, leaving a wide gap between the edges of the central domain. *WOX3*, *WUSCHEL-LIKE HOMEOBOX3*.

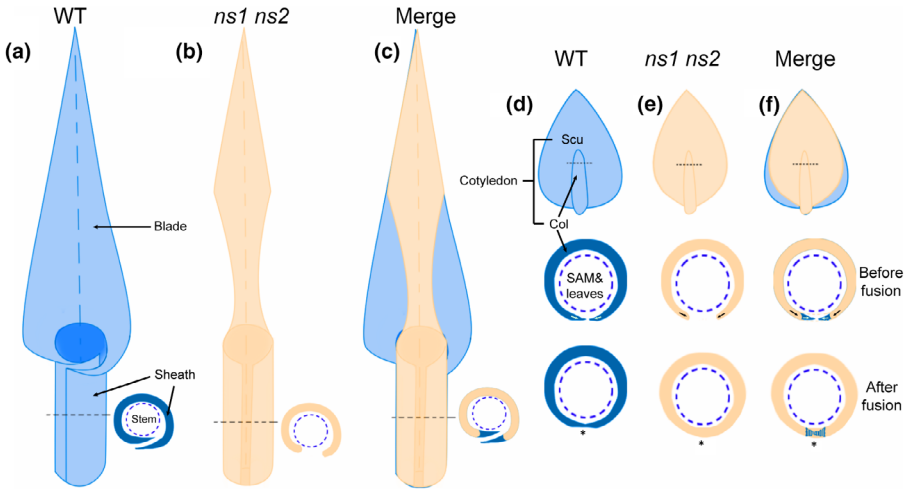


**Fig. 7** Model for homology of the bipartite grass cotyledon comprising a distal scutellum and the proximal coleoptile. (a–c) Mutations in the duplicate genes *ns1* and *ns2* cause narrow leaves by deleting a leaf domain that extends from the proximal half of the leaf blade and includes the entire length of the sheath, thereby preventing the leaf sheath from wrapping around the stem. The blue parts of the merged leaf image (c) are deleted in the *ns* double mutant (b). (d–f) Equivalent phenotypes are seen in *ns1 ns2* mutant embryos, where the *ns* domain deletion (shown in blue in the merged cartoons) affects just the proximal base of the scutellum (Scu) but the entire length of the coleoptile (Col). Note that although the *ns1 ns2* double-mutant coleoptile margins do eventually fuse, the marginal domains are deleted (blue in (f) after fusion), leaving the champagne colored domains in both leaves (b, c) and embryo (e, f).

scutellum and coleoptile are partially conjoined, unlike those of the coleoptile and the first leaf or any two successive grass leaves, thereby suggesting a unified, single cotyledon. In this view, some morphologists have argued that the scutellum comprises the apical region of the maize cotyledon, whereas the coleoptile forms its sheathing base (Fig. 7). The scutellum initiates before the coleoptile (Abbe & Stein, 1954), and lineage analyses of clonal sectors, analyses of leaf initiation inhibitors, and pseudotime analyses of maize leaf differentiation all support hypotheses where the maize leaf blade initiates before the leaf sheath; newly initiated leaf primordia comprise cells that are mostly fated to become leaf blade, and the most proximal domains of the maize sheath do not emerge from the shoot until the leaf is the fourth primordium from the SAM (Poethig, 1984; Scanlon, 2003; Satterlee *et al.*, 2020).

Expression of leaf developmental markers and the *ns1 ns2* double-mutant phenotypes suggest that the scutellum and coleoptile are indeed leaf homologs, although these leaf patterning transcripts are not detected in later stages of scutellum development when its morphology is distinctly divergent from that of foliar leaves. Grass leaves contain a distal, photosynthetic leaf blade and a proximal sheath surrounding the stem. We note that the *ns1 ns2* double-mutant leaf phenotype extends the entire length of the sheath, but this marginal leaf-domain deletion affects just the proximal region of the leaf blade (Fig. 7a–c; Scanlon *et al.*, 1996). The leaf tip is unaffected in *ns1 ns2* double mutants and resembles that of WT siblings. As shown in Fig. 2(a, b) and modeled in Fig. 7(d–f), the scutellum of *ns1 ns2* double-mutant seed is similarly affected only in the proximal regions, whereas the tip of the scutellum is unaffected. By contrast, the marginal domain deletion in the *ns1 ns2* double mutant extends the entire length of the truncated, yet fused mutant coleoptile, which is equivalent to the phenotype observed in the leaf sheath that fails to surround the stem (Fig. 7b; Scanlon *et al.*, 1996).

Thus, these genetic analyses of higher-order *wox3* mutations support a bipartite model of the grass cotyledon, as comprising the fusion of a distal, haustorial scutellum and a proximal, sheathing coleoptile. In the same way that the grass leaf comprises a distal blade fused to a proximal sheath to form a single lateral organ (phytomer), we propose that the grass cotyledon comprises a distal scutellum and a proximal coleoptile fused to form a single cotyledon. We propose that the grass embryo evolved this bipartite cotyledon morphology where the haustorial scutellum digests nutrient reserves within the endosperm to nourish the foliar leaves before they emerge from the plumule as autotrophic photosynthetic organs, whereas the sheathing coleoptile is emergent and protects these tender embryonic leaves during germination through the soil.

These data support morphological models, wherein grasses and palms, with large and persistent endosperms, have evolved haustorial cotyledons (i.e. the scutellum) that remain underground with the seed while the base of this single cotyledon forms a sheathing, leaf-like structure that emerges from the soil at germination (Campbell, 1930; Kaplan & Specht, 2022). Several species of *Peperomia* have one haustorial cotyledon fused to the seed and a second cotyledon that emerges as a foliar leaf, suggesting a model for monocotyledon evolution wherein the two cotyledons of the dicot ancestor had adapted to acquire two very different functions and were later united to form a single organ in the monocotyledons (Hill, 1906). Moreover, Campbell (1930) reported several examples among the eudicot *Ranunculaceae* where the two cotyledons are united, including cases where the proximal cotyledon undergoes marginal fusion to form a cylindrical sheath. Taken together, our morphological, developmental genetic, and gene expression analyses support a model where the scutellum and the coleoptile comprise the single, bipartite, grass cotyledon.

## Acknowledgements

We thank Weill Growth Chamber facilities and the Cornell Gutermann Greenhouse facilities for plant care. HW was supported by a grant from the National Science Foundation (IOS-2016021). RZ is supported by another grant from the National

Science Foundation (IOS-2210259). We are grateful for comments from L. Evans and R. Ragas on the data and the manuscript.

## Competing interests

None declared.

## Author contributions

MJS and HW planned and designed the research. HW and RZ performed experiments and analyzed the data. HW performed all genetic crosses and generated original artwork. MJS, RZ and HW wrote the manuscript.

## ORCID

Michael J. Scanlon https://orcid.org/0000-0003-1708-3490
Ruqiang Zhang https://orcid.org/0000-0002-6459-7294

## Data availability

All mutant maize lines utilized in this study are available from the Maize Genetics Cooperation Stock Center, located at the University of Illinois, Urbana/Champaign (http://maizecoop.cropsci.uiuc.edu/). All Xenium™ multiplex *in situ* hybridization data are deposited in Science Data Bank with the link: https://www.scidb.cn/s/F7ZbEz; visualization utilizes Xenium Explorer v.1.3, as described in Wu *et al.* (2024). All other data materials utilized in this paper are included in the article figures and Fig. S1.

## References

**Abbe EC, Stein OL. 1954.** The growth of the shoot apex in maize: embryogeny. *American Journal of Botany* **41**: 285–293.

**Anderson MJ. 2001.** A new method for non-parametric multivariate analysis of variance: non-parametric ANOVA for ecology. *Austral Ecology* **26**: 32–46.

**Bossinger G, Lundquist U, Salamini F. 1992.** Genetics of plant development in barley. *Barley Genetics* **2**: 989–1022.

**Boyd L. 1931.** Evolution in the monocotyledonous seedling: A new interpretation of the morphology of the grass embryo. *Transactions of the Botanical Society of Edinburgh* **30**: 286–303.

**Burger WC. 1998.** The question of cotyledon homology in angiosperms. *Botanical Review* **64**: 356–371.

**Campbell DH. 1930.** The phylogeny of monocotyledons. *Annals of Botany* **44**: 311–331.

**Chandler JW. 2008.** Cotyledon organogenesis. *Journal of Experimental Botany* **59**: 2917–2931.

**Claude J. 2008.** *Morphometrics with R.* New York, NY, USA: Springer.

**Cronquist A. 1988.** *The evolution and classification of flowering plants, 2nd edn.* New York, NY, USA: New York Botanical Garden.

**Dean E. 2002.** Upcoming changes in flowering plant family names: those pesky taxonomists are at it again! *Fremontia* **30**: 3–12.

**Fu YB. 2024.** Polycotyly: how little do we know? *Plants* **13**: 1054.

**Haines RW, Lye KA. 1979.** Monocotylar seedlings: a review of evidence supporting an origin by fusion. *Botanical Journal of the Linnaean Society* **78**: 123–140.

**Hill AW. 1906.** The morphology and seedling structure of the geophilous species of peperomia, together with some views on the origin of monocotyledons. *Annals of Botany* **20**: 395–427.

**Iwata H, Ukai Y. 2002.** SHAPE: a computer program package for quantitative evaluation of biological shapes based on elliptic Fourier descriptors. *The Journal of Heredity* **93**: 384–385.

**Jackson D. 1991.** *In situ* hybridization in plants. In: Bowles DJ, Gurr SJ, McPherson M, eds. *Molecular plant pathology: a practical approach.* Oxford, UK: Oxford University Press.

**Kaplan DR. 1984.** *Cladistics: perspectives on the reconstruction of evolutionary history.* New York, NY, USA: Columbia University Press.

**Kaplan DR, Cooke TJ. 1997.** Fundamental concepts in the embryogenesis of dicotyledons: a morphological interpretation of embryo mutants. *Plant Cell* **9**: 1903–1919.

**Kaplan DR, Specht CD. 2022.** *Kaplan's principles of plant morphology.* New York, NY, USA: CRC Press.

**Kausch AP, Wang K, Kaeppler HF, Gordon-Kamm W. 2021.** Maize transformation: history, progress, and perspectives. *Molecular Breeding* **41**: 38.

**Kiesselbach TA. 1949.** The structure and reproduction of corn. *University of Nebraska Agriculture of Statistic Research Bulletin* **161**: 1–96.

**Langdale JA, Zelitch I, Miller E, Nelson T. 1988.** Cell position and light influence $C_4$ versus $C_3$ patterns of photosynthetic gene expression in maize. *EMBO Journal* **7**: 3643–3651.

**Leiboff S, DeAllie CK, Scanlon MJ. 2016.** Modeling the morphometric evolution of the maize shoot apical meristem. *Frontiers in Plant Science* **7**: 1651.

**Nardmann J, Ji J, Werr W, Scanlon MJ. 2004.** The maize duplicate genes narrow sheath1 and narrow sheath2 encode a conserved homeobox gene function in a lateral domain of shoot apical meristems. *Development* **131**: 2827–2839.

**Niklas KJ. 2008.** Embryo morphology and seedling evolution. In: Leck MA, ed. *Seedling ecology and evolution.* Cambridge, UK: Cambridge University Press, 103–129.

**Poethig RS. 1984.** Cellular parameters of leaf morphogenesis in maize and tobacco. In: White R, Dickison W, eds. *Contemporary problems in plant anatomy.* New York, NY, USA: Academic Press, 235–238.

**Ray J. 1686.** *Historia plantarum.* London, UK: The Royal Society.

**Rohatgi A. 2022.** *WebPlotDigitizer (v.4.6).* [WWW document] URL https://automeris.io/WebPlotDigitizer.html [accessed 16 September 2022].

**Sargent E. 1903.** A theory of the origin of monocotyledons found on the structure of their seedlings. *Annals of Botany* **17**: 1–92.

**Satterlee JW, Evans LJ, Conlon BR, Conklin P, Martinez-Gomez J, Yen JR, Wu H, Sylvester AW, Specht CD, Cheng J *et al.* 2023.** A Wox3-patterning module organizes planar growth in grass leaves and ligules. *Nature Plants* **9**: 720–732.

**Satterlee JW, Strable J, Scanlon MJ. 2020.** Plant stem-cell organization and differentiation at single-cell resolution. *Proceedings of the National Academy of Sciences, USA* **117**: 33689–33699.

**Scanlon MJ. 2003.** The polar auxin transport inhibitor N-1-naphthylphthalamic acid disrupts leaf initiation, KNOX protein regulation, and formation of leaf margins in maize. *Plant Physiology* **133**: 597–605.

**Scanlon MJ, Freeling M. 1998.** The narrow sheath leaf domain deletion : a genetic tool used to reveal developmental homologies among modified maize organs. *The Plant Journal* **13**: 547–561.

**Scanlon MJ, Schneeberger RG, Freeling M. 1996.** The maize mutant narrow sheath fails to establish leaf margin identity in a meristematic domain. *Development* **122**: 1683–1691.

**Schnable PS, Ware D, Fulton RS, Stein JC, Wei F, Pasternak S, Liang C, Zhang J, Fulton L, Graves TA *et al.* 2009.** The B73 maize genome: complexity, diversity, and dynamics. *Science* **26**: 1112–1115.

**Strable J, Yen JR, Scanlon MJ, Sylvester AW. 2020.** Toluidine Blue O staining of paraffin-sectioned maize tissue. *Bio-Protocol* **101**: e3612.

**Takacs EM, Li J, Du C, Ponnala L, Janick-Buckner D, Yu J, Muehlbauer GJ, Schnable PS, Timmermans MC, Sun Q *et al.* 2012.** Ontogeny of the maize shoot apical meristem. *Plant Cell* **24**: 3219–3234.

**Tillich HJ. 1990.** The seedlings of Nymphaeaceae: monocotylar or dicotylar? *Flora* **184**: 169–176.

**Titova GE, Batygina TB. 1986.** Is the embryo of Nymphaealean plants (Nymphaeales s.l.) dicotyledonous? *Phytomorphology* **46**: 171–190.

**Tomlinson PB. 2016.** *The botany of mangroves.* Cambridge, UK: Cambridge University Press.

**Vollbrecht E, Reiser L, Hake S. 2000.** Shoot meristem size is dependent on inbred background and presence of the maize homeobox gene, knotted1. *Development* **127**: 3161–3172.

**Weatherwax P. 1920.** Position of scutellum and homology of coleoptile in maize. *Botanical Gazette* **69**: 179–182.

**Wu H, Zhang R, Scanlon MJ. 2024.** A multiplexed transcriptomic analysis of a plant embryonic hourglass. *BioRxiv*. doi: 10.1101/2024.04.04.588207.

## Supporting Information

Additional Supporting Information may be found online in the Supporting Information section at the end of the article.

**Fig. S1** Seedling coleoptile phenotypes of the *wox3* higher-order mutants.

Please note: Wiley is not responsible for the content or functionality of any Supporting Information supplied by the authors. Any queries (other than missing material) should be directed to the *New Phytologist* Central Office.